# Gas slippage effect on microscale porous flow using the lattice Boltzmann method

G. H. Tang,* W. Q. Tao, and Y. L. He
*State Key Laboratory of Multiphase Flow, School of Energy and Power Engineering, Xi'an Jiaotong University, Xi'an, Shaanxi 710049, China*
(Received 26 June 2005; published 1 November 2005)

A lattice Boltzmann method is developed for gaseous slip flow at the pore scale in microscale porous geometries. Flow characteristics through various porous structures are studied for different Knudsen numbers and inlet to outlet pressure ratios. It is found that the gas permeability is larger than the absolute permeability of porous media due to the gas slippage effect. Furthermore, the rarefaction influence on the gas permeability is more evident for porous structures with low porosity. The Klinkenberg equation is confirmed for the simulated porous structures. However, the second-order term of the Knudsen number ($Kn^2$) cannot be neglected for gaseous flow with relatively high Knudsen numbers. A model for predicting the pressure drop of the flow through microscale porous media is presented based on the Ergun equation and the Carman-Kozeny equation by taking into account the effects of gas rarefaction and compressibility.

DOI: 10.1103/PhysRevE.72.056301 PACS number(s): 47.11.+j, 47.55.Mh, 47.45.Gx

## I. INTRODUCTION

The study of the physics of flow through porous media has become basic to many applied scientific and engineering fields. Such diversified fields as soil mechanics, groundwater hydrology, petroleum engineering, water purification, industrial filtration, ceramic engineering, powder metallurgy, and the study of gas marks all rely heavily on it as fundamental to their individual problems [1].

Porous flow problems are usually treated by volume-averaged approaches. For the case of a single viscous fluid flowing through porous media, Darcy's flow is often used for calculating the volume rate per unit area in these structures. Darcy's law is valid for flows with Reynolds numbers less than one, in which the convective term in the Navier-Stokes equation is negligible. For higher Reynolds numbers, the Ergun equation based on experimental data is often used [2]. With these approaches, one can obtain macroscopic properties of flow in porous media. Because of the very complicated boundaries in pore structures, a macroscopic framework cannot provide exact solutions of flow through porous media and diffusion in pores. Lattice gas automata and lattice Boltzmann methods (LBM) have been shown to have the capability of solving these problems. The main advantage of the lattice Boltzmann method is that the method has strong flexibility for complex geometries.

However, to the authors' knowledge, the existing LBM models for porous media are all based on the continuum assumption. Rothman [3], one of the first researchers, used the lattice gas automata to simulate two-dimensional flow through porous media. Chen *et al.* [4] and Cancelliere *et al.* [5] used the lattice gas automata for two- and three-dimensional simulations. Adrover and Giona [6], and Koponen *et al.* [7,8] used the LBM for two-dimensional porous structures. Succi *et al.* [9], Heijs and Lowe [10], Maier *et al.* [11], and Inamuro *et al.* [12] simulated three-dimensional porous structures with the LBM. The reliability of the LBM in modeling fluid flow in porous media was confirmed in these studies. Recent researches on continuum single-phase flow in simple or complicated porous media can see Refs. [13–19]. Guo and Zhao [20] also studied the porous media flow at the representative elementary volume scale with the LBM. But for microscale and nanoscale pores encountered in many applications, the pore size is so small that the gaseous flow through these structures may fall into slip or transition regime. In fact, gas slippage effect on the permeability of tight sands [21–25] and nanostructures [26] has been observed in experiments. Thus, it is quite necessary to develop a lattice Boltzmann model for microscale porous applications. This paper presents such a work for simulating gas flow in porous media at the microscale level. This paper is organized as follows. Section II derives the permeability expression for gas flow in ideal cases consisting of parallel microtube bundle. Section III introduces the LBM model for microscale porous media. Section IV presents typical numerical results of velocity vector, volume flow rate, permeability, and pressure drop in microscale porous media using the presented D2Q9 lattice BGK model. Section V concludes the paper.

## II. GAS PERMEABILITY IN MICROCHANNELS AND MICROTUBES

First, let us review some knowledge of the rarefied gas dynamics. The Knudsen number, which is defined as $Kn=\lambda/H$ [27], provides a direct means of validating the continuum approach as it compares the mean free path, $\lambda$, to the characteristic height, $H$. A flow is considered as a continuum for $Kn<0.001$. For $Kn>10$ the system can be considered as a free molecular flow and the direct simulation of Monte Carlo method is usually used for simulating such flows. The intermediate values of $0.1<Kn<10$ are associated with a transition flow regime while those within the range of $0.001<Kn<0.1$ are representative of a slip flow regime. Navier-Stokes equation with slip velocity boundary may be

*Email address: ghtang@mail.xjtu.edu.cn

 

TABLE I. Coefficients for various second-order slip models.

| Author(s) | $C_1$ | $C_2$ |
|---|---|---|
| Schamberg [28] | 1.0 | $5\pi/12$ |
| Cercignani [29] | 1.1466 | 0.9756 |
| Deissler [30] | 1.0 | 9/8 |
| Sreekanth [31] | 1.1466 | 0.14 |
| Hisa and Domoto [32] | 1.0 | 0.5 |
| Mitsuya [33] | 1.0 | 2/9 |
| Beskok *et al.* [34] | 1.0 | −0.5 |

applied to flows within the slip regime or marginally transition regime.

Consider two-dimensional isothermal gas flow between parallel plates. The channel with the height of $H$ extends from $y=0$ to $y=H$. If the Reynolds number is relatively low, the inertial terms in the Navier-Stokes equation are neglected and the momentum equation takes the following form for fully developed flow:

$$\frac{d^2u}{dy^2} = \frac{1}{\mu}\frac{dp}{dx}, \tag{1}$$

where $\mu$ is the dynamic viscosity of the fluid. The boundary conditions are

$$u = \pm C_1\lambda\frac{\partial u}{\partial y} - C_2\lambda^2\frac{\partial^2 u}{\partial y^2}, \tag{2}$$

where $C_1$ and $C_2$ are coefficients denoting the first-order term and second-order term, respectively. The values of $C_1$ and $C_2$ [28–34] are summarized in Table I. Then, we can obtain the following streamwise velocity profile in the channel with a second-order slip velocity boundary condition

$$u(y) = -\frac{H^2}{2\mu}\frac{dp}{dx}\left(\frac{y}{H} - \frac{y^2}{H^2} + C_1\mathrm{Kn} + 2C_2\mathrm{Kn}^2\right). \tag{3}$$

Integration in $y$-coordinate results in an expression for the average velocity in the channel

$$q = u_A = -\frac{H^2}{2\mu}\frac{dp}{dx}\left(\frac{1}{6} + C_1\mathrm{Kn} + 2C_2\mathrm{Kn}^2\right). \tag{4}$$

As all known, in one-dimensional system, Darcy's law is given by the following equation

$$q = -\frac{k}{\mu}\frac{dp}{dx}, \tag{5}$$

where $q$ is the volume flow rate per unit area, $k$ is the permeability of the porous structure, and $dp/dx$ is the applied pressure gradient. In comparison with Eq. (5), the following formula can be derived from Eq. (4)

$$k = \frac{H^2}{12}(1 + 6C_1\mathrm{Kn} + 12C_2\mathrm{Kn}^2). \tag{6}$$

Thus, for rarefied gaseous flow in a parallel channel, the permeability is dependent not only on the channel characteristic height but also on the Knudsen number. For continuum flow at $\mathrm{Kn}=0$, we have $k=H^2/12$ and the permeability only depends on the characteristic height. Similarly, for rarefied gaseous flow in a microtube with diameter $D$, we can obtain the following permeability expression:

$$k = \frac{1}{32}D^2(1 + 8C_1\mathrm{Kn} + 16C_2\mathrm{Kn}^2). \tag{7}$$

Considering an ideal porous media composed of a bundle of straight and parallel circular tubes of equal diameters $D$ and $N$ tubes per unit cross-sectional area of the porous media, the permeability velocity is calculated as

$$q = N\frac{\pi D^2}{4}u_A = -\frac{N\pi D^4}{128\mu}\frac{dp}{dx}(1 + 8C_1\mathrm{Kn} + 16C_2\mathrm{Kn}^2). \tag{8}$$

The mean free path $\lambda$ is defined [27]

$$\lambda = \frac{\mu}{\bar{p}}\sqrt{\frac{\pi RT}{2}}, \tag{9}$$

where $R$ is the gas constant, $T$ is the temperature, and $\bar{p}$ is the mean pressure of the channel inlet and outlet. Thus we can obtain

$$q = -\frac{N\pi D^4}{128\mu}\frac{dp}{dx}\left(1 + \frac{8\mu}{D}\sqrt{\frac{\pi RT}{2}}C_1\frac{1}{\bar{p}} + \frac{8\pi RT\mu^2}{D^2}C_2\frac{1}{\bar{p}^2}\right). \tag{10}$$

Thus the gas permeability can be written as

$$k_g = k_\infty\left(1 + \frac{A}{\bar{p}} + \frac{B}{\bar{p}^2}\right), \tag{11}$$

where $k_\infty$ is the absolute permeability, or permeability unaffected by the gas slippage

$$k_\infty = \frac{N\pi D^4}{128}, \tag{12a}$$

$$A = \frac{8\mu}{D}\sqrt{\frac{\pi RT}{2}}C_1, \tag{12b}$$

$$B = \frac{8\pi RT\mu^2}{D^2}C_2. \tag{12c}$$

For a real porous structure, different coefficients should be added before the above three terms. According to Klinkenberg, gas permeability at a finite pressure is given by [35]

$$k_g = k_\infty\left(1 + \frac{A}{\bar{p}}\right). \tag{13}$$

Note that the second-order correction in Eq. (11), $B/\bar{p}^2$, has the same action with the first-order term if $C_2$ is positive. Indeed, $C_2$ is positive for most of the second-order slip boundary models (see Table I). The effect of the second-order term can account for the deviation from a straight line for the curve relating $k_g$ and $1/\bar{p}$ observed in the core sample experiment [36]. The gas permeability with different experiment pressure is plotted in Fig. 1. The second-order term

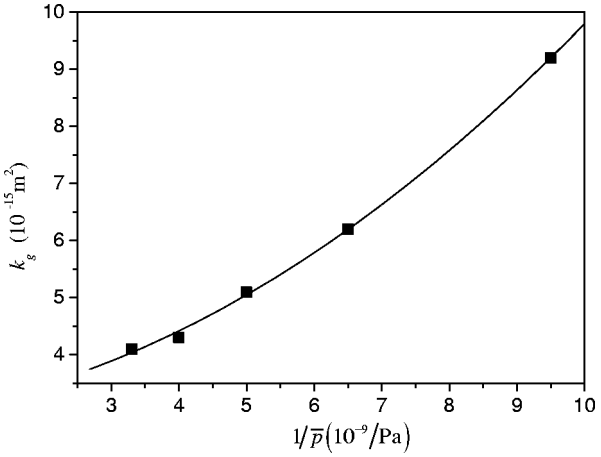


FIG. 1. Plot of experimental gas permeability and reciprocal mean pressure.

effect will be significant especially for very small pores or large Knudsen numbers.

## III. LATTICE BOLTZMANN METHOD FOR MICROSCALE POROUS MEDIA

The lattice Boltzmann method, which was developed from the lattice gas automata, simulates fluid flows by tracking the evolution of fluid particles taken on a few discrete speeds in discrete space at discrete time steps. The LBM method has been mainly applied to the continuum flow since its birth. Very recently, the LBM has been successfully developed to simulate microflows [37–41]. In this paper, we applied the LBM model developed in our recent work [39] to investigate the transport characteristics in microscale porous media.

The kinetic evolution of the lattice Boltzmann equation with the BGK collision approximation is [42]

$$f_i(\mathbf{r}+\mathbf{c}_i\Delta t, t+\Delta t) = f_i(\mathbf{r},t) - \frac{1}{\tau}[f_i(\mathbf{r},t) - f_i^{eq}(\mathbf{r},t)], \quad (14)$$

where $\tau$ is the dimensionless relaxation time. For the D2Q9 lattice model, the discrete velocities are given by $\mathbf{c}_0=0$, and $\mathbf{c}_i=(\cos[(i-1)\pi/2], \sin[(i-1)\pi/2])c$ for $i=1,2,3,4$, and $\mathbf{c}_i=\sqrt{2}(\cos[(i-5)\pi/2+\pi/4], \sin[(i-5)\pi/2+\pi/4])c$ for $i=5,6,7,8$. The streaming speed, $c$, is defined as $\Delta x/\Delta t$, where $\Delta x$ and $\Delta t$ are the lattice spacing and time step, respectively.

The equilibrium distribution function $f_i^{eq}$ for the D2Q9 model is

$$f_i^{eq} = \rho\omega_i\left[1 + \frac{3(\mathbf{c}_i\cdot\mathbf{u})}{c^2} + \frac{9(\mathbf{c}_i\cdot\mathbf{u})^2}{2c^4} - \frac{3(\mathbf{u}\cdot\mathbf{u})}{2c^2}\right], \quad (15)$$

where $\omega_0=4/9$, $\omega_i=1/9$ for $i=1,2,3,4$, and $\omega_i=1/36$ for $i=5,6,7,8$. The macroscopic variables for the fluid mass density, fluid momentum, and pressure are defined by $\rho=\Sigma_i f_i$, $\rho\mathbf{u}=\Sigma_i f_i\mathbf{c}_i$, and $p=\rho c^2/3$. The term $\tau$ in Eq. (14) is replaced by $\tau'$ to take into account the gas compressibility [39],

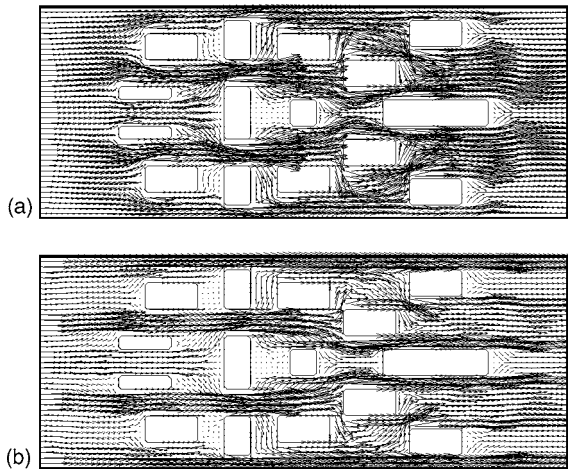


FIG. 2. Velocity vectors in the porous structure of $\varepsilon=0.825$ at $p_i/p_o=1.1$. (a) $\mathrm{Kn}_o=0.055$. (b) $\mathrm{Kn}_o=0.16$.

$$\tau' = \frac{1}{2} + \frac{\rho_{ref}}{\rho}\left(\tau - \frac{1}{2}\right), \quad (16)$$

where $\rho_{ref}$ is a referenced density and $\tau$ is linked with the channel outlet Knudsen number $\mathrm{Kn}_o$ via the following equation [39]

$$\tau = \frac{\rho_o N_y \mathrm{Kn}_o}{\rho_{ref}\sqrt{\pi/6}} + \frac{1}{2}, \quad (17)$$

where $\rho_o$ is the outlet gas density and $N_y$ is the characteristic lattice number. In this modified lattice Boltzmann model, we can obtain the fluid dynamic viscosity $\mu$ independent of the density as the following expression [39]:

$$\mu = \frac{(\tau-0.5)\Delta t\rho_{ref}c^2}{3}. \quad (18)$$

The slip velocities on all the solid block surfaces and the plate wall boundaries are implemented by combining the bounce-back with the specular reflection [39].

## IV. SIMULATION RESULTS

The simulated 2D porous media is like the structure shown in Fig. 2. Disordered solid blocks are packed between two parallel plates. Porosity $\varepsilon$ represents the fraction void volume in the porous structure and it is defined as $\varepsilon=(V-V_s)/V$, where $V$ is the total volume, and $V_s$ is the volume of the solid blocks. Isothermal gaseous flows in such microscale porous structures are simulated with the presented lattice Boltzmann method. The height of the simulated channels is $H=1.2$ $\mu$m and the ratio of the channel length, $L$, to the height is 2.5. The channel outlet is fixed at atmospheric condition. The working fluids of carbon dioxide ($CO_2$), nitrogen ($N_2$), hydrogen ($H_2$), and helium (He) are simulated, and the corresponding outlet Knudsen numbers are 0.0236, 0.055, 0.1, and 0.16, respectively. In the simulations, we maintain a pressure difference by holding a fixed density at the inlet and outlet.

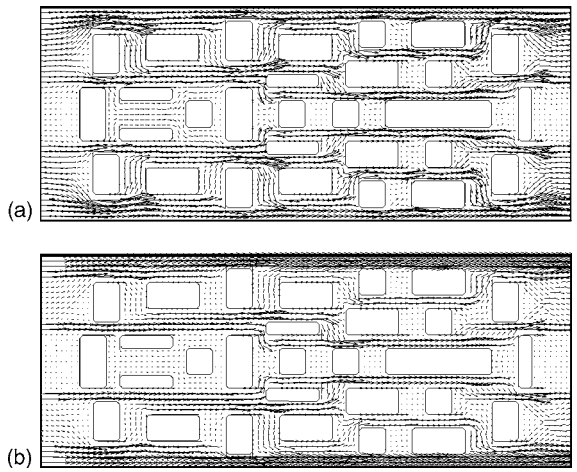


FIG. 3. Velocity vectors in the porous structure of $\varepsilon=0.719$ at $p_i/p_o=1.1$. (a) $\mathrm{Kn}_o=0.055$. (b) $\mathrm{Kn}_o=0.16$.

### A. Velocity profiles

The calculated results of velocity vectors for different values of porosity at pressure ratio of the inlet to outlet $p_i/p_o=1.1$ are shown in Figs. 2 and 3, where the length of the vectors stands for the magnitude of the velocity. It is seen that at a higher Knudsen number, $\mathrm{Kn}_o=0.16$, the slip velocities on the bottom and top plates are much larger than those at $\mathrm{Kn}_o=0.055$. Conversely, the velocities away from the plates are lower. Moreover, due to the reduced friction drag on the plates at larger Knudsen number, the flow rate gets higher near plates and lower among the disordered blocks, which makes flow separations behind the blocks unlikely to occur. In other words, if the Reynolds number increases, the vortices behind the disordered blocks are more inclined to occur at relatively low Knudsen numbers. Thus the pressure drag acting on the solid blocks increases and the fluid flows away from the blocks into open spaces near flat plates with smaller pressure drags. Seen from Fig. 3, as the porosity decreases, the flow resistance increases and the flow velocity through the porous structure decreases obviously.

### B. Volume flow rate and permeability

A plot of volume flow rate per unit area as a function of the pressure difference between the inlet and outlet for six values of porosity $\varepsilon=0.887$, 0.869, 0.825, 0.769, 0.719, and 0.675 is shown in Figs. 4(a) and 4(b). The results can be well fitted by a series of straight lines. The Knudsen number has significant influence on the flow rate. As seen from the figures, at the same pressure gradient, the volume flow rate increases with the increase of Knudsen number, implying the reduction in friction drags on the walls and blocks. The flow rate decreases steeply with the increasing porosity. However, for porous structures with relatively small porosity, the flow rate is affected to a less degree than those having higher levels of porosity. For example, as shown in Figs. 4(a) and 4(b), the flow rate discrepancy is relatively small between $\varepsilon=0.719$ and $\varepsilon=0.675$.

The average gas permeability is evaluated from pressure and flow data using a non-Klinkenberg gas flow solution of compressible gas [1]

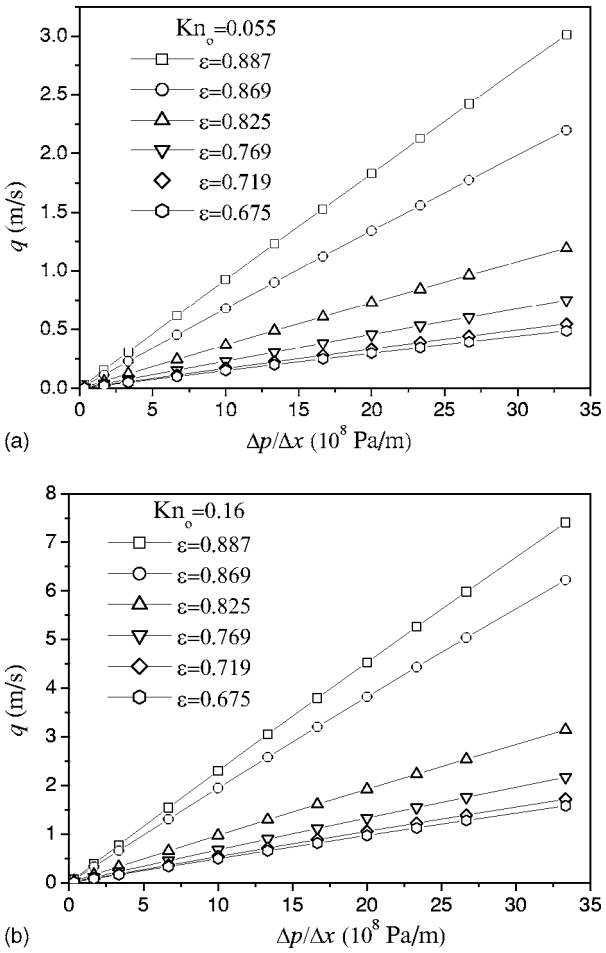


FIG. 4. The volume flow rate $q$ as a function of the pressure gradient for various porosities and Knudsen numbers. (a) $\mathrm{Kn}_o=0.055$. (b) $\mathrm{Kn}_o=0.16$.

$$k_g=\frac{2\mu L q_o p_o}{p_i^2-p_o^2}, \tag{19}$$

where $p_i$, $p_o$, and $q_o$ are the inlet pressure, outlet pressure, and outlet velocity, respectively.

The gas permeability is shown in Fig. 5 as a function of the reciprocal mean pressure, $1/\bar{p}$. From the figure we can see that the gas permeability decreases evidently as the mean pressure increases, especially for relatively high Knudsen numbers. However, the influence is weak for a small Knudsen number, that is, for a near continuum flow. Note that the rarefaction effect is expected to decrease with the increasing pressure because the mean free path $\lambda$ of the gas is inversely proportional to the pressure $p$. The Knudsen number increases from the inlet to outlet as the pressure decreases in the streamwise direction, reaching a maximum at the outlet of the channel. In our simulation the outlet condition is fixed at atmosphere. Thus, as the mean pressure increases, the inlet pressure increases and the degree of the whole rarefaction level in the porous structure decreases, which results in relatively large flow resistance and consequently low gas permeability.

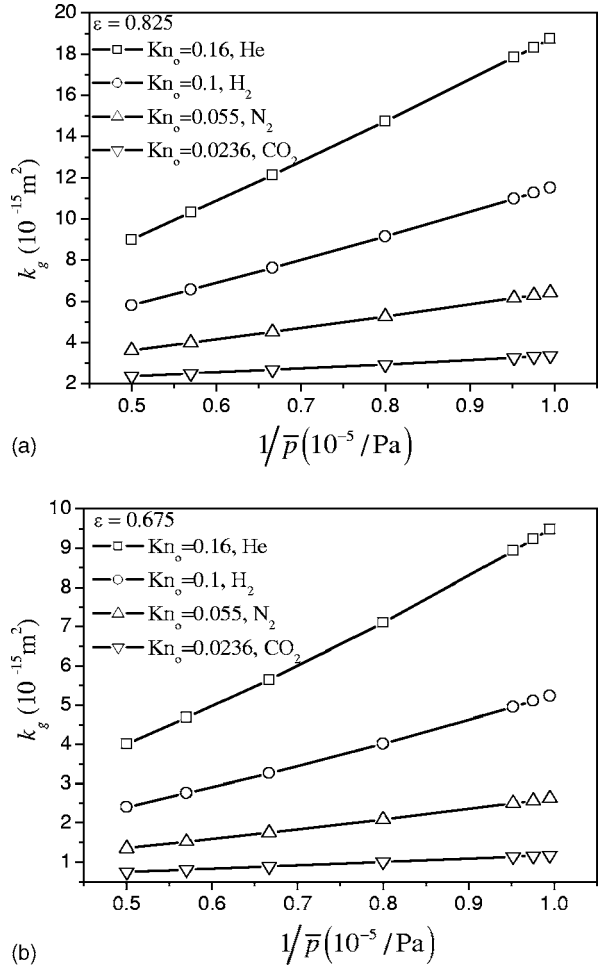


FIG. 5. The Knudsen number influence on gas permeability. (a) $\varepsilon=0.825$. (b) $\varepsilon=0.675$.

Because of the gas slippage on the solid boundaries, the friction drag reduces and thus the permeability increases with the increasing Knudsen number. Similar experimental results for $H_2$, $N_2$, and $CO_2$ flows through a porous medium are presented in Ref. [43]. One can also see Ref. [44] for details. The simulated results from the presented LBM method are consistent with the experimental data qualitatively.

On the whole, the simulation results can be quite well fitted by a series of straight lines. The slop of the straight line relating the gas permeability to reciprocal mean pressure decreases with the increasing Knudsen numbers. Nevertheless, by careful inspection of the results, it can be observed that the predicted gas permeability slightly deviates from the straight line for helium flow shown in Fig. 5(b). This deviation is attributed to the effect of the second-order term of Knudsen number.

The calculated results of gas permeability for the porous structures with $\varepsilon=0.825$ and $\varepsilon=0.675$ at $\bar{p}=1.05\times10^5$ Pa are listed in Table II. The gas permeability for the porous structure with $\varepsilon=1.0$ (no solid blocks between the two parallel plates) is also listed in Table II. We find that as the porosity decreases, the Knudsen number influence on the gas permeability becomes more evident. For example, for the porous structure with $\varepsilon=1.0$, the permeability of helium flow ($\mathrm{Kn}_o=0.16$) is 1.9 times larger than that of carbon dioxide flow ($\mathrm{Kn}_o=0.0236$), while it is 5.4 times larger for the porous structure with $\varepsilon=0.825$ and 7.8 times larger for the porous structure with $\varepsilon=0.675$, respectively. This simulation result is consistent with the experimental data in Refs. [21,22,25]. This characteristic can be explained as follows: as the porosity decreases, generally the total surface area of the solid blocks increases and the slippage effect on the solid surfaces becomes more dominant, which results in a lower flow resistance through the porous structure. This result means that the neglect of gas rarefaction effect would bring forth large deviation from the true transport characteristics, especially for the porous media with low porosity.

### C. Pressure drops

Finally, we compare the calculated results of pressure drops with the following empirical equations based on experimental data, the Ergun correlation of Eq. (20) [2] and the Carman-Kozeny correlation of Eq. (21) [45]

$$\frac{\Delta p}{L}\frac{D_p}{\rho u^2}\frac{\varepsilon^3}{1-\varepsilon}=150\frac{\mu(1-\varepsilon)}{\rho u D_p}+1.75, \tag{20}$$

$$\frac{\Delta p}{L}\frac{D_p}{\rho u^2}\frac{\varepsilon^3}{1-\varepsilon}=180\frac{\mu(1-\varepsilon)}{\rho u D_p}. \tag{21}$$

Figure 6 shows the dimensionless pressure drops versus the Reynolds numbers multiplied by $1/(1-\varepsilon)$ for the porous structure of $\varepsilon=0.675$, where $\bar{\rho}_i$ and $\bar{u}_i$ represent the inlet mean density and velocity, respectively. First, we tried to determine the value of the equivalent diameter of the body, $D_p$, by comparing the calculated pressure drop with the Carman-Kozeny equation and the Ergun equation. We simulated the flow at $\mathrm{Kn}_o=0.001$ since it can be considered as a continuum flow. We found that a good agreement is obtained with $D_p=0.16$ $\mu$m by comparing the calculated results with the above two empirical equations. The dimensionless pres-

TABLE II. The gas permeability for various Knudsen numbers and porosities at $\bar{p}=1.05\times10^5$ Pa.

| | $\varepsilon=1.0$ | $\varepsilon=0.825$ | $\varepsilon=0.675$ |
|---|---|---|---|
| $\mathrm{Kn}_o=0.0236$ | $1.21\times10^{-13}$ m$^2$ | $3.26\times10^{-15}$ m$^2$ | $1.14\times10^{-15}$ m$^2$ |
| $\mathrm{Kn}_o=0.055$ | $1.48\times10^{-13}$ m$^2$ | $6.52\times10^{-15}$ m$^2$ | $2.5\times10^{-15}$ m$^2$ |
| $\mathrm{Kn}_o=0.1$ | $1.8\times10^{-13}$ m$^2$ | $10.97\times10^{-15}$ m$^2$ | $4.95\times10^{-15}$ m$^2$ |
| $\mathrm{Kn}_o=0.16$ | $2.3\times10^{-13}$ m$^2$ | $17.84\times10^{-15}$ m$^2$ | $8.94\times10^{-15}$ m$^2$ |

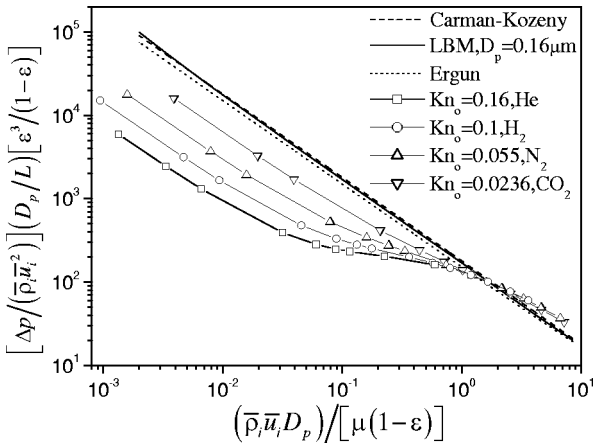


FIG. 6. Pressure drops versus Reynolds numbers in the porous structure of $\varepsilon=0.675$. The ordinate is $[\Delta p/(\bar{\rho}_i\bar{u}_i^2)](D_p/L)[\varepsilon^3/(1-\varepsilon)]$.

sure drops are lower than the Ergun equation for the other four Knudsen numbers at lower Reynolds numbers in Fig. 6. However, the discrepancies between the four gases get lower and eventually the dimensionless pressure drops exceed the Ergun equation at larger Reynolds numbers. As previously mentioned, as the Reynolds number increases, the inlet pressure increases and the mean Knudsen number of the inlet and the outlet decreases. That is, the mean Knudsen number discrepancies are small between the four gas flows at higher inlet pressures, which results in the quite close pressure drops. However, it is difficult to explain that the pressure drops exceed the continuum Ergun equation. We recall that the Ergun equation and the Carman-Kozeny equation are limited to near incompressible flow. Thus, considering the gas compressibility and comparing Eq. (5) with Eq. (19), we rewrite the ordinate as shown in Fig. 7. From Fig. 7 we can see that the pressure drops are always below the continuum Ergun equation. To fit the data for different Knudsen numbers with a single straight line, we rewrite the ordinate again by multiplying $(1+A\,\overline{\mathrm{Kn}})$ as shown in Fig. 8. Here $\overline{\mathrm{Kn}}$ is the mean Knudsen number of the inlet and outlet and $A$ is a

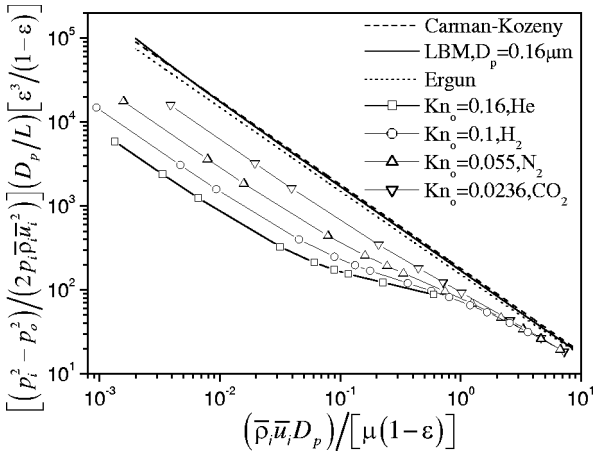


FIG. 7. Pressure drops considering the compressibility versus Reynolds numbers in the porous structure of $\varepsilon=0.675$. The ordinate is $[(p_i^2-p_o^2)/(2p_i\bar{\rho}_i\bar{u}_i^2)](D_p/L)[\varepsilon^3/(1-\varepsilon)]$.

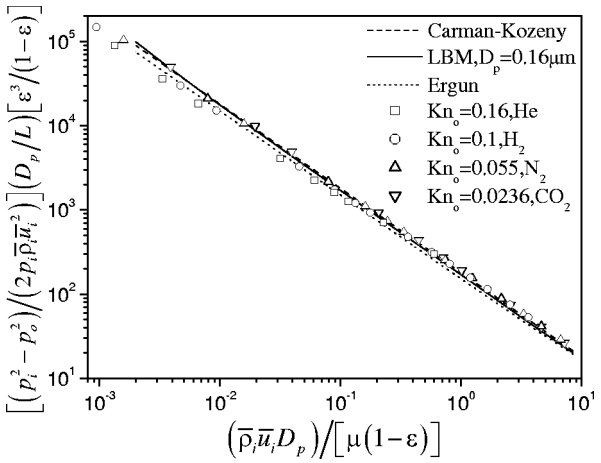


FIG. 8. Pressure drops considering the compressibility and rarefaction versus Reynolds numbers in the porous structure of $\varepsilon=0.675$. The ordinate is $[(p_i^2-p_o^2)/(2p_i\bar{\rho}_i\bar{u}_i^2)](D_p/L)[\varepsilon^3/(1-\varepsilon)](1+A\,\overline{\mathrm{Kn}})$.

constant. The data are in good agreement with the Ergun equation and the Carman-Kozeny equation if $A$ is set to be 90. However, at lower Reynolds numbers for helium flow, corresponding to lower inlet pressures, a slight lower deviation can still be observed due to the larger mean Knudsen number. Namely, the second-order term of Knudsen number cannot be neglected at larger Knudsen numbers. If one still adopts a first-order correlation to fit the data, one must increase the value of factor $A$, which means that the factor $A$ would not be expected to be a constant in the whole Knudsen number regime even for the same porous structure. In other words, the factor $A$ depends on the porous properties, as well as, to a lesser degree, on the nature of the gas used. Similarly, by comparing the pressure drops at $\mathrm{Kn}_o=0.001$ with the Ergun equation and the Carman-Kozeny equation, we determined the values of $D_p$ to be 0.12, 0.14, and 0.14 for the porous structures of $\varepsilon=0.825$, $\varepsilon=0.769$, and $\varepsilon=0.719$, respectively. Using the first-order correlation, we determined the value of constant $A$ to be 55, 60, and 80, respectively. It can be seen that the value of constant $A$ increases as the porosity decreases. The results are presented in Fig. 9 for $CO_2$, $N_2$, $H_2$, and He flows in the four porous structures of $\varepsilon=0.825$, 0.769, 0.719, and 0.675. The four solid lines represent the results at $\mathrm{Kn}_o=0.001$ (continuum flow) and they accord with each other perfectly. We can see that the dots and the solid lines are in good agreement except at very low Reynolds numbers, where the second order of Knudsen number effect is evident.

## V. CONCLUSIONS

Analytical solution for gas permeability through an ideal porous structure consisting of a bundle of microtubes is presented, which provides a supplement for Klinkenberg equation by introducing a second-order correction, $B/\bar{p}^2$. A lattice Boltzmann model is presented which can take into account the influence of gas rarefaction. The transport characteristics in relatively simple porous structures are studied with the

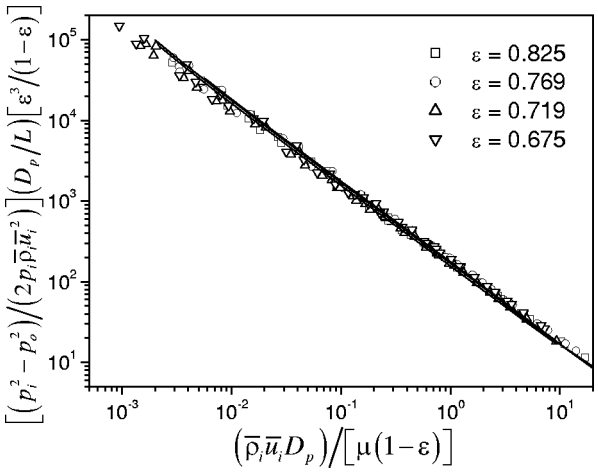


FIG. 9. Pressure drops versus Reynolds numbers for the four porous structures of $\varepsilon$=0825, 0.769, 0.719, and 0.675 with four different gas flows. The four solid lines represent the results at $\mathrm{Kn}_o$=0.001 and they accord with each other perfectly. The dots indicate the simulation results of $CO_2$, $N_2$, $H_2$, and He flows at the four porous structures.

presented LBM method. The results show that the Knudsen number has significant influence on the gas permeability. For the same porous structure, the permeability increases with the increase of Knudsen number. A qualitatively good agreement is obtained between the simulated results and the experimental data.

Considering the compressibility and the rarefaction, a model for the pressure drop is presented based on the Ergun equation and the Carman-Kozeny equation. By introducing a correlation about the first-order Knudsen number, the Ergun equation is still applicable for moderate Knudsen number range. However, the second-order Knudsen number effect cannot be neglected for high Knudsen number flows.

The gaseous rarefaction effect on the gas permeability is more evident for the porous structure with low porosity. The conventional continuum models for transport characteristics study in microscale porous media are not valid or at least should be modified. The lattice Boltzmann method can reveal not only the local behavior but also integral quantities like the pressure drop. It is demonstrated to be an effective method for simulating complicated phenomena of gas flow through porous media.

Finally, note that the pore size is different in the whole porous media and thus the local Knudsen number varies from pore to pore. Further developments of the present work should include the effect of the variation of the local Knudsen number.

## ACKNOWLEDGMENTS

This work was supported by the National Natural Science Foundation of China (Grant Nos. 50406020 and 50425620) and the National Fundamental Research Program of China (Grant No. 2006CB601203).

[1] A. E. Scheidrgger, *The Physics of Flow Through Porous Media*, 3rd ed. (University of Toronto Press, Toronto, 1972).
[2] S. Ergun, Chem. Eng. Prog. **48**, 89 (1952).
[3] D. H. Rothman, Geophysics **53**, 509 (1988).
[4] S. Chen, K. Diemer, G. D. Doolen, K. Eggert, C. Fu, S. Gutman, and B. J. Travis, Physica D **47**, 72 (1991).
[5] A. Cancelliere, C. Chang, E. Foti, D. H. Rothman, and S. Succi, Phys. Fluids A **2**, 2085 (1990).
[6] A. Adrover and M. Giona, Chem. Eng. J. **64**, 7 (1996).
[7] A. Koponen, M. Kataja, and J. Timonen, Phys. Rev. E **56**, 3319 (1997).
[8] A. Koponen, M. Kataja, J. Timonen, and D. Kandhai, Int. J. Mod. Phys. C **9**, 1505 (1998).
[9] S. Succi, R. Benzi, and H. Francisco, Physica D **47**, 219 (1991).
[10] A. W. J. Heijs and C. P. Lowe, Phys. Rev. E **51**, 4346 (1995).
[11] R. S. Maier, D. M. Kroll, Y. E. Kutsovsky, H. T. Davis, and R. S. Bernard, Phys. Fluids **10**, 60 (1998).
[12] T. Inamuro, M. Yoshino, and F. Ogino, Int. J. Numer. Methods Fluids **29**, 737 (1999).
[13] D. S. Clague, B. D. Kandhai, R. Zhang, and P. M. A. Sloot, Phys. Rev. E **61**, 616 (2000).
[14] M. Singh and K. K. Mohanty, Chem. Eng. Sci. **55**, 5393 (2000).
[15] J. Kim, J. Lee, and K. C. Lee, Physica A **293**, 13 (2001).
[16] E. S. Boek, J. Chin, and P. V. Coveney, Int. J. Mod. Phys. B **17**, 99 (2003).
[17] Q. H. Kang, D. X. Zhang, and S. Y. Chen, Phys. Rev. E **66**, 056307 (2002).
[18] S. J. Humby, M. J. Biggs, and U. Tuzun, Chem. Eng. Sci. **57**, 1955 (2002).
[19] H. Freund, T. Zeiser, F. Huber, E. Klemm, G. Brenner, F. Durst, and G. Emig, Chem. Eng. Sci. **58**, 903 (2003).
[20] Z. Guo and T. S. Zhao, Phys. Rev. E **66**, 036304 (2002).
[21] F. O. Jones and W. W. Owens, JPT, J. Pet. Technol. **32**, 1631 (1980).
[22] K. Sampath and C. W. Keighin, JPT, J. Pet. Technol. **34**, 2715 (1982).
[23] T. Ertekin, G. R. King, and F. C. Schwerer, SPE Form. Eval. **1**, 43 (1986).
[24] H. Loosveldt, Z. Lafhaj, and F. Skoczylas, Cem. Concr. Res. **32**, 1357 (2002).
[25] P. Persoff and J. B. Hulen, Geothermics **30**, 169 (2004).
[26] V. Lysenko, J. Vitiello, B. Remaki, and D. Barbier, Phys. Rev. E **70**, 017301 (2004).
[27] S. A. Schaaf and P. L. Chambre, *Flow of Rarefied Gases* (Princeton University Press, Princeton, NJ, 1961).
[28] R. Schamberg, Ph.D. thesis, California Institute of Technology, Pasadena, 1947.
[29] C. Cercignani, Institute of Engineering Research Report AS-64–19, University of California, Berkeley, 1964.
[30] R. G. Deissler, Int. J. Heat Mass Transfer **7**, 681 (1964).

[31] A. K. Sreekanth, in *Proceedings of the 6th International Symposium on Rarefied Gas Dynamics*, edited by L. Trilling and H. Y. Wachman (Academic Press, New York, 1969), Vol. 1, pp. 667–680.
[32] Y. T. Hisa and G. A. Domoto, ASME J. Lubr. Technol. **105**, 120 (1983).
[33] Y. Mitsuya, J. Tribol. **115**, 289 (1993).
[34] A. Beskok, G. E. Karniadakis, and W. Trimmer, ASME J. Fluids Eng. **118**, 448 (1996).
[35] L. J. Klinkenberg, *The Permeability of Porous Media to Liquids and Gases* (American Petroleum Inst., Drilling and Productions practices, New York, 1941).
[36] Y. J. Wang, C. J. Wang, and J. B. Gao, Acta Petrolei Sinica **16**, 101 (1995) (in Chinese).
[37] X. B. Nie, G. D. Doolen, and S. Y. Chen, J. Stat. Phys. **107**, 279 (2002).
[38] C. Y. Lim, C. Shu, X. D. Niu, and Y. T. Chew, Phys. Fluids **14**, 2299 (2002).
[39] G. H. Tang, W. Q. Tao, and Y. L. He, Int. J. Mod. Phys. C **15**, 335 (2004).
[40] G. H. Tang, W. Q. Tao, and Y. L. He, Phys. Fluids **17**, 058101 (2005).
[41] Y. Zhang, R. Qin, and D. R. Emerson, Phys. Rev. E **71**, 047702 (2005).
[42] S. Succi, *Lattice Boltzmann Equation for Fluid Dynamics and Beyond* (Clarendon Press, Oxford, 2001).
[43] J. L. Ge, *Porous Flow Mechanics in Gas and Oil Reservoir* (Petroleum Industry Press, Beijing, 1982) (in Chinese).
[44] G. H. Tang, W. Q. Tao, and Y. L. He, J. Appl. Phys. **97**, 104918 (2005).
[45] J. Bear, *Dynamics of Fluids in Porous Media* (Elsevier Publishing Company, Amsterdam, 1972).